Human Molecular Genetics, 2011, Vol. 20, No. 4 ***719–730***
doi:10.1093/hmg/ddq517
Advance Access published on December 1, 2010

Decreased catalytic activity and altered activation properties of PDE6C mutants associated with autosomal recessive achromatopsia

Tanja Grau[1], Nikolai O. Artemyev[2], Thomas Rosenberg[3,4], Hélène Dollfus[5], Olav H. Haugen[6], E. Cumhur Sener[7], Bernhard Jurklies[8], Sten Andreasson[9], Christoph Kernstock[10], Michael Larsen[3,11], Eberhart Zrenner[10], Bernd Wissinger[1] and Susanne Kohl[1,*]

[1]Molecular Genetics Laboratory, Institute for Ophthalmic Research, Centre for Ophthalmology, University Clinics Tuebingen, Roentgenweg 11, D-72076 Tuebingen, Germany, [2]Department of Molecular Physiology and Biophysics, University of Iowa College of Medicine, 51 Newton Road, Iowa City, IA 52242-1109, USA, [3]National Eye Clinic and [4]The Gordon Norrie Centre for Genetic Eye Disease, Kennedy Center, DK-2600 Glostrup, Denmark, [5]Centre de reference pour les Affections Rare en Génétique Ophthalmologique, Hôpitaux Universitaires de Strasbourg, 1 place de ÍHôpital, 67000 Strasbourg, France, [6]Department of Ophthalmology, Haukeland University Hospital, N-5021 Bergen, Norway, [7]Department of Ophthalmology, Hacettepe University, Shhiye-Ankara 06100, Turkey, [8]University Eye Hospital Essen, Hufelandstrasse 55, D-45122 Essen, Germany, [9]Department of Ophthalmology, University Hospital of Lund, 22185 Lund, Sweden, [10]Division of Experimental Ophthalmology, Institute for Ophthalmic Research, University Tuebingen, Schleichstrasse 12-16, D-72076 Tuebingen, Germany and [11]Department of Ophthalmology, Glostrup Hospital and Kennedy Center, National Eye Clinic, University of Copenhagen, Nordre Ringvej 57, DK-2600 Glostrup, Denmark

Received October 7, 2010; Revised November 18, 2010; Accepted November 24, 2010

Mutations in the gene encoding the catalytic subunit of the cone photoreceptor phosphodiesterase (*PDE6C*) have been recently reported in patients with autosomal recessive inherited achromatopsia (ACHM) and early-onset cone photoreceptor dysfunction. Here we present the results of a comprehensive study on *PDE6C* mutations including the mutation spectrum, its prevalence in a large cohort of ACHM/cone dysfunction patients, the clinical phenotype and the functional characterization of mutant PDE6C proteins. Twelve affected patients from seven independent families segregating *PDE6C* mutations were identified in our total patient cohort of 492 independent families. Eleven different *PDE6C* mutations were found including two nonsense mutations, three mutations affecting transcript splicing as shown by minigene assays, one 1 bp-insertion and five missense mutations. We also performed a detailed functional characterization of six missense mutations applying the baculovirus system to express recombinant mutant and wildtype chimeric PDE6C/PDE5 proteins in Sf9 insect cells. Purified proteins were analyzed using Western blotting, phosphodiesterase (PDE) activity measurements as well as inhibition assays by zaprinast and Pγ. Four of the six *PDE6C* missense mutations led to baseline PDE activities and most likely represent functional null alleles. For two mutations, p.E790K and p.Y323N, we observed reduction in PDE activity of approximately 60% and 80%, respectively. We also observed differences for Pγ inhibition. The p.E790K mutant, with an IC_{50} value of 2.7 nM is 20.7-fold more sensitive for Pγ inhibition, whereas the p.Y323N mutant with an IC_{50} of 158 nM is 3-fold less sensitive when compared with the wildtype control.

INTRODUCTION

Light detection in the human retina mediated by rod and cone photoreceptors is a complex signal transduction process. Hereby, the photoreceptor phosphodiesterases (PDE6) play a key role by rapidly decreasing intracellular levels of the second messenger cGMP in the outer segment. Upon light stimulation,

*To whom correspondence should be addressed. Tel: +49 7071 29 80702; Fax: +49 7071 29 5725; Email: susanne.kohl@uni-tuebingen.de

the photopigment is excited and in this state activates the G-protein transducin through GDP/GTP exchange and release of the Gα-subunit (Tα). The latter binds and displaces the inhibitory γ-subunit (Pγ) of the PDE6 (1). This step activates the catalytic PDE6 dimer that rapidly hydrolyzes intracellular cGMP molecules, resulting in the closure of cGMP-gated channels and hyperpolarization of the photoreceptor plasma membrane. cGMP levels are quickly recovered by synthesis through guanylyl cyclases to re-establish the dark-adapted state (1). Rod and cone photoreceptors employ the same biochemical mechanism, yet the molecular components are unique and specific for either rods or cones. For instance, in rods, a rod-specific Pγ blocks the activity of the heterodimeric PDE6αβ catalytic core. Cone PDE in contrast is composed of a cone-specific PDEα′ homodimer, complexed with two cone-specific Pγ subunits. Each PDE6 subunit in the catalytic dimer possesses two regulatory GAF domains located at the N-terminal part of the protein and one conserved C-terminal PDE catalytic domain (2,3). Functional investigation of PDE6 has been hampered by the failure of recombinant protein expression in bacteria and mammalian cell lines. Therefore, chimeric fusion proteins between PDE6C and the ubiquitously expressed PDE5 have been developed that overcomes this problem (4–6). PDE5 and PDE6C are quite similar in terms of domain organization. Both have two N-terminal GAF domains and one catalytic domain located in the C-terminal part of the molecules. In addition, PDE5 and PDE6 share a relatively high homology of the catalytic domains, specificity to cGMP and sensitivity to common catalytic-site inhibitors, such as sildenafil, zaprinast and IBMX (4).

Loss or dysfunction of any component of the phototransduction cascade results in photoreceptor degeneration and visual function loss in human. Achromatopsia (ACHM) (MIM *600827) is a congenital or early-onset retinal disorder with cone photoreceptor function loss. Inherited as an autosomal recessive trait, ACHM is characterized by reduced visual acuity, a pendular nystagmus, photophobia, small central scotoma, eccentric fixation and reduced or complete loss of color discrimination. In photopic electroretinographic recordings (ERG), the cone response is absent or markedly diminished, whereas the scotopic rod response is essentially normal. In rare cases, an incomplete form of ACHM can be observed with similar but less severe symptoms. While mutations in *CNGA3* (MIM *600053), *CNGB3* (MIM *605080) and *GNAT2* (MIM +139340) are well-documented causes of ACHM (7–13), very recently mutations in *PDE6C* have been identified in patients with this disease (14,15).

Here we report the results of our comprehensive study on *PDE6C* mutations including new mutations and a complete mutation spectrum, the prevalence of *PDE6C* mutations in our cohort of 492 independent ACHM patients/families, the clinical phenotype and detailed functional characterization of six *PDE6C* missense mutations introduced into chimeric PDE6C/PDE5 enzyme.

RESULTS

Identification of *PDE6C* mutations

Microsatellite marker analysis for the known ACHM loci was performed in 16 families with at least two affected siblings or evidence of parental consanguinity. Among those, five families (CHRO 9, CHRO 102, CHRO 566, CHRO 572 and CHRO 573) were found to show concordant segregation for the *PDE6C* locus. Screening of the *PDE6C* gene by sequencing all coding exons in the index patients revealed the presence of compound heterozygous or homozygous mutations in four of these families. In addition to the previously reported mutations in family CHRO 9 [compound heterozygous for c.481-12T>A and c.1483-2A>G, (15)], family CHRO 102 [compound heterozygous for c.1805A>T/p.H602L and c.2368G>A/p.E790K, (15)] and CHRO 572 [homozygous for c.1682_1683insA/p.Y561X, (15)], we found a novel homozygous missense mutation, c.310C>T/p.R104W, in family CHRO 573 (Fig. 1A). All missense mutations affect amino acid residues highly conserved among different species and PDE6 isoforms (Supplementary Material, Figure S1).

We then extended our mutation screening to include another 77 independent index patients who did not carry mutations in *CNGA3* and *CNGB3*. In addition to CHRO 287, which was found to be compound heterozygous for two nonsense mutations [c.826C>T/p.R276X and c.2457T>A/p.Y819X, (15)], we found two further patients with mutations in *PDE6C*: CHRO 319 was compound heterozygous for c.85C>T/p.R29W and c.2144+1G>A, and CHRO 403 homozygous for the missense mutation c.1172C>T/p.P391L (Fig. 1A and Table 1). All mutations showed consistent independent segregation in the respective families.

Minigene assays of putative splicing mutation

All three putative splicing mutations and the c.2368G>A mutation, which represents a substitution of the first nucleotide of exon 21 were analyzed by heterologous splicing assays of minigene constructs in COS7 cells. In addition to the previously reported defects in transcript splicing induced by the c.481-12T>A, the c.1483-2A>G and the c.2368G>A mutations (15), we also observed a splice defect with minigene constructs carrying the c.2144+1G>A mutation. In this case, a cryptic splice site four nucleotides downstream of the genuine 5′ splice donor site is activated, which results in a frame-shift and the introduction of a premature termination codon (p.M715IfsX2) (Fig. 1B).

Functional effects of *PDE6C* missense mutations

PDE activity. To investigate the functional consequences of *PDE6C* missense mutations, we generated a ‘humanized’ chimeric PDE6C/PDE5 construct for recombinant protein expression in Sf9 insect cells. In addition to the five missense mutations identified in our study, we also included the p.Y323N mutation, reported by Thiadens and co-workers (14) (Fig. 2). Purified wildtype and mutant chimeric proteins were analyzed for catalytic activity (cGMP hydrolysis) and inhibition by zaprinast and Pγ. Four of the mutant proteins (p.R29W, p.R104W, p.P391L and p.H602L) showed only minute catalytic activity that ranged between 4.5% and 8.6% of the normalized chimeric wildtype protein activity. In contrast, we observed considerable residual enzymatic activity for the p.E790K and the p.Y323N mutants. The p.E790K amino acid substitution is located within the catalytic

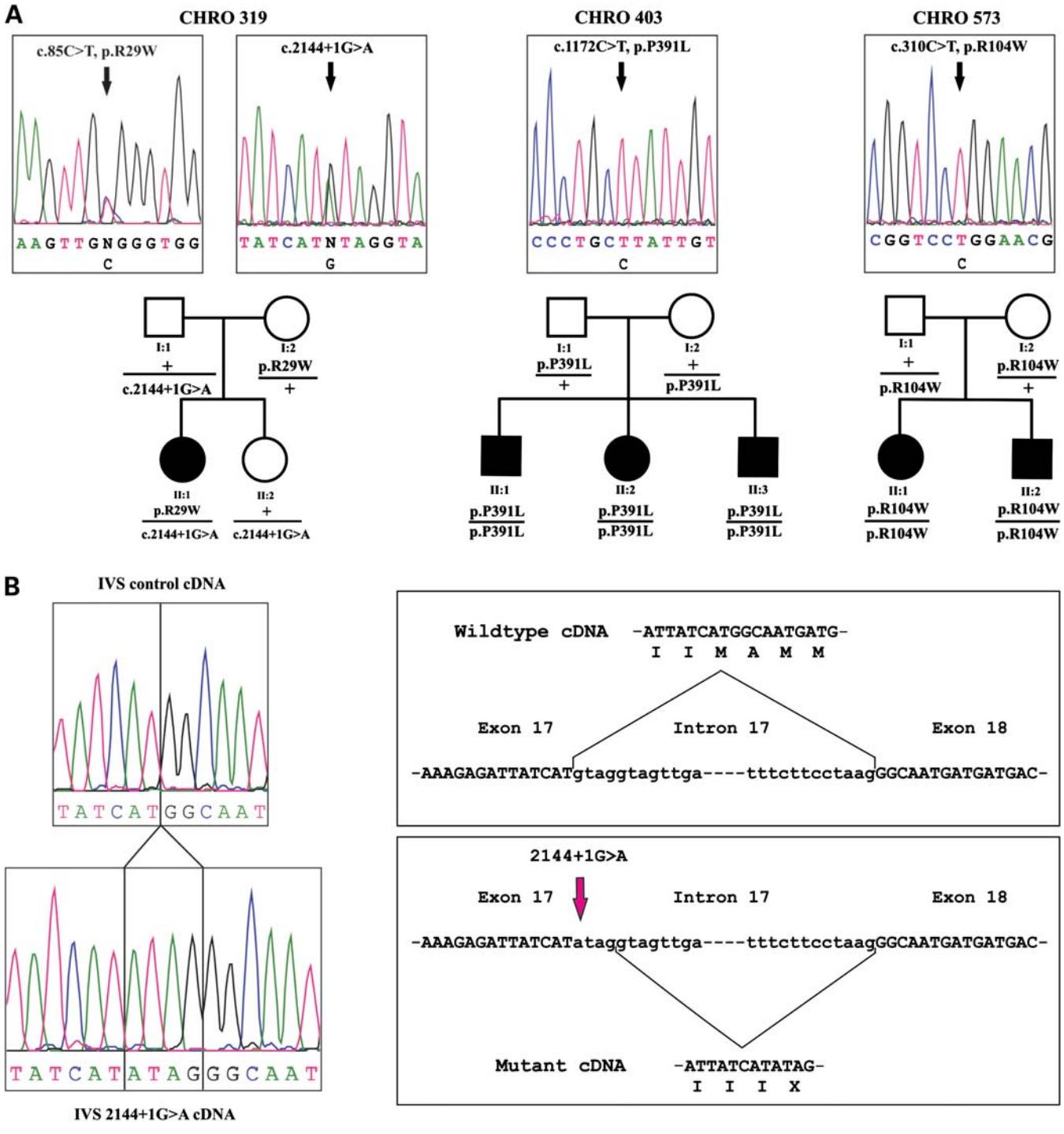

Figure 1. (**A**) *PDE6C* mutations in ACHM patients and segregation analysis. Sequence traces of all identified mutations (top) and their segregation in the respective families (bottom) are displayed. (**B**) Heterologous splicing assay of the c.2144+1G>A mutation. Sequence sections of RT–PCR products from RNA of COS7 cells transfected with either mutant (bottom) or wildtype constructs (top), and schematic overview of the deduced processing of wildtype and mutant transcripts. Expression of an exon 16–18 minigene construct in COS7 cells revealed the activation of a cryptic splice site in the c.2144+1G>A construct. The mis-spliced cDNA carries a frame-shift followed by a premature termination codon.

domain of PDE6, in the vicinity of the inhibitory PDEγ-binding region. For this mutant, a residual activity of approximately 40% compared with wildtype was measured (15) (Fig. 3 and Table 2). The p.Y323N substitution localizes within the non-catalytic GAFb domain, known to have regulatory function. In comparison with the normalized wildtype activity, this mutant showed a residual enzyme activity of 22.3%. The mutants p.Y323N and p.E790K were then

Table 1. *PDE6C* mutations and allelic composition in ACHM patients identified in this study

Family	Allele 1 Nucleotide level	Protein level	Allele 2 Nucleotide level	Protein level
CHRO 9[a]	c.481-12T>A	Splice defect	c.1483-2A>G	Splice defect
CHRO 102[a]	c.1805A>T	p.H602L	c.2368G>A	p.E790K
CHRO 287[a]	c.826C>T	p.R276X	c.2457T>A	p.Y819X
CHRO 319	c.85C>T	p.R29W	c.2144+1G>A	Splice defect
CHRO 403	c.1172C>T	p.P391L	c.1172C>T	p.P391L
CHRO 572[a]	c.1682_1683insA	p.Y561X	c.1682_1683insA	p.Y561X
CHRO 573	c.310C>T	p.R104W	c.310C>T	p.R104W

[a]Published in Chang *et al*. (15)

further analyzed for the kinetics of the enzymatic activity in comparison with the chimeric wildtype protein. The wildtype PDE6C/PDE5 protein hydrolyzed cGMP with a K_m value of 0.72 μM and a k_{cat} value of 0.12 s^{-1} (Fig. 4A and Table 2). For the p.E790K mutant as well as the p.Y323N mutant, we obtained K_m values of 0.53 and 0.56 μM, and k_{cat} values of 0.065 and 0.035 s^{-1}, respectively. For both mutants, the K_m values were comparable to those of the wildtype PDE6C/PDE5, whereas statistically significant differences ($P < 0.001$) in k_{cat} values for both mutants were obtained.

PDE inhibition

Inhibition of the mutants by zaprinast. Zaprinast, a competitive inhibitor specific for PDE6 and PDE5, was used to further investigate the properties of the catalytic pocket of the p.E790K and p.Y323N mutants in comparison with the wildtype PDE6C/PDE5 (Fig. 4C and Table 2). Zaprinast inhibited cGMP hydrolysis of the wildtype PDE6C/PDE5 with an IC_{50} value of 2.9 μM. In comparison with that, we obtained a 2.4-fold increased zaprinast sensitivity for the p.E790K ($IC_{50} = 1.2$ M), and a 2.8-fold reduced inhibitory effect of zaprinast on the p.Y323N ($IC_{50} = 8.1$ M) mutant.

Inhibition of the mutants by Pγ. Dose–response relationships for inhibition of cGMP hydrolytic activity by Pγ were measured for the chimeric wildtype and the two mutants p.E790K and p.Y323N that showed residual enzymatic activity (Fig. 3 and Table 2). Pγ inhibited the chimeric wildtype with an IC_{50} value of 56 nM (Fig. 4B). The IC_{50} value of 158 nM for the p.Y323N was approximately 3-fold higher when compared with wildtype, whereas for the p.E790K mutant an IC_{50} value of 2.7 nM was obtained. The 20.7-fold shift of the dose–response curve towards lower Pγ concentrations for p.E790K proved to be statistically significant ($P = 0.004$). The p.E790K substitution remarkably increases the ability of Pγ to inhibit the enzyme activity.

Patients' phenotypes. Clinical data were available for all 12 patients with mutations in *PDE6C* (Table 3). All patients had a clinical diagnosis of ACHM, and a family history compatible with an autosomal recessive trait. Ophthalmoscopic fundus appearance was unremarkable in most subjects, but some patients showed atrophy of the retinal pigment epithelium (RPE) or granular pigmentation in the macula. Two examples for fundus photography and optical coherence tomography (OCT) are shown for a 33-year-old woman (CHRO 319/II:1—Fig. 5A–D) and a 14-year-old boy (CHRO 287/II:1—Fig. 5E–G). Fundus examination was unremarkable in both patients (Fig. 5), except for a thin, pale line outlining a circular area of 250 μm diameter around the foveola in the right eye of patient CHRO319/II:1 (Fig. 5A) and a central cystic macular lesion in both eyes of patient CHRO 287/II:1 (Fig. 5E and F). On transfoveal scans, an optically empty cavity was seen in both patients (250 μm diameter for patient CHRO 319/II:1; 720 μm diameter for patient CHRO 287/II:1) above the RPE, corresponding to discontinuity of the photoreceptor layer in the central circular area of the fovea, extending to the internal limiting membrane (Fig. 5D and G).

Mutation spectrum and prevalence of PDE6C mutations in ACHM patients. From this study and the previous report by Thiadens and co-workers (14), 16 different pathogenic mutations in *PDE6C* are known to date (Fig. 2). This includes nine protein truncation mutations (three nonsense mutations, one frame-shift mutation and five splice site mutation producing aberrant transcripts with altered reading frame), but also seven missense mutations. Two mutations c.85C>T/p.R29W and c.310C>T/p.R104W were found in exon 1, and c.310C>T/p.R104W localizes in the GAFa domain. The c.967T>A/p.Y323N mutation in exon 6 and the c.1172C>T/p.P391L mutation in exon 9 are situated in the second regulatory GAFb domain, while the c.1363A>G/p.M455V mutation in exon 10 is closely behind that. Two mutations c.1805A>T/p.H602L in exon 14 and c.2368G>A/p.E790K in exon 21 affect the catalytic PDEaseI domain (Fig. 2). Except for the c.85C>T/p.R29W mutation, which has been found in this study as well as in the study of Thiadens and co-workers (14), all other mutations were only detected in single families.

Currently our cohort comprises 492 independent patients and families with a clinical diagnosis of autosomal recessive ACHM. Approximately 77% of these patients carry mutations in either *CNGA3* ($n = 141$ patients; 28.7%) or *CNGB3* ($n = 237$ patients; 48.2%), the by far most prevalent gene mutated in ACHM (10,16, unpublished data). Mutations in *GNAT2* and *PDE6C* are much less prevalent in our cohort (*GNAT2*—11 families, ((12), unpublished results) and *PDE6C*—seven families, this study) with a prevalence of 2.2% and 1.4%, respectively.

DISCUSSION

In this paper we compiled all data of our study on *PDE6C* mutations including new mutations and a complete mutation spectrum, the prevalence of *PDE6C* mutations in our cohort of 492 independent ACHM patients and families, the clinical phenotype and a detailed functional characterization of *PDE6C* missense mutations using purified recombinant protein. For the latter, we investigated two novel *PDE6C*

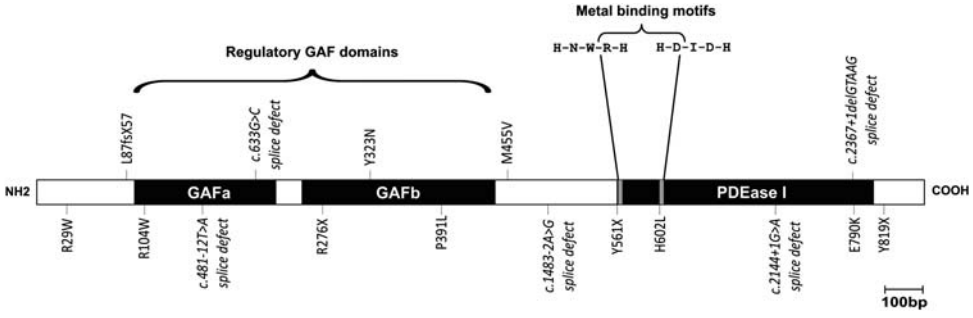

Figure 2. Overview of the localization of all currently known *PDE6C* mutations, including seven missense mutations, five splice defects, three nonsense and one frame-shift mutations.

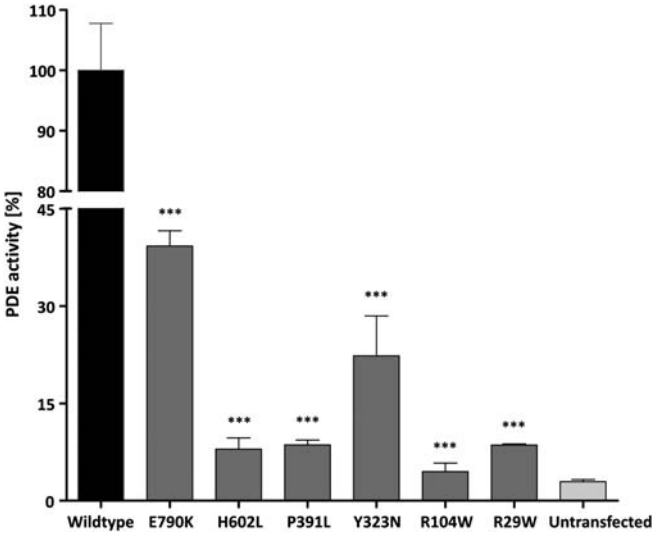

Figure 3. Reduced or loss of catalytic activity of mutant PDE6C/PDE5 chimeras. Equal amounts of purified protein were assayed for cGMP hydrolysis activity. Activities were normalized to the wildtype protein. Untransfected Sf9 insect cells were measured as control for intrinsic PDE activity. For the p.E790K mutant, we obtained activity of approximately 40% and for the p.Y323N mutant, a reduction in PDE activity of around 78%. All the other mutants p.H602L, p.P391L, p.R104W and p.R29W showed only low PDE activity not significantly different from the untransfected control. Triple asterisk (***) indicates highly significant difference ($P < 0.001$) in the catalytic activity between wildtype and mutant protein.

missense mutations (p.R104W and p.P391L) as well as four previously described amino acid substitutions (p.R29W, p.Y323N, p.H602L and p.E790K), all identified in human subjects with autosomal recessively inherited ACHM (14,15). Up to now, no disease-associated *PDE6C* mutation had been functionally characterized in detail, leaving uncertainty about the pathogenicity of these missense mutations. The results of our functional analyses now confirm that all six missense mutations are in fact pathogenic. Four mutations (p.R29W, p.R104W, p.P391L and p.H602L) showed highly significant reduction in PDE activity, to almost baseline levels, and are unlikely to mediate any cone function under physiological conditions. For two mutations, p.E790K and p.Y323N, we observed highly significant reduction in PDE activity of approximately 60% and 80%, respectively.

The missense mutation p.R29W was observed in one ACHM family in our study and has also been reported by Thiadens and co-workers, in this case in homozygous state (14). It localizes near the N-terminus of cone PDE6 upstream of the GAFa domain, and affects an amino acid that is conserved among vertebrate PDE6C and PDE6A polypeptides, except for bovine PDE6C (Supplementary Material, Figure S1). For this mutant, we observed a complete loss of enzymatic function. In previous studies it has been shown that dimerization of PDE6 is mediated by multiple regions in the N-terminal domain (17). We therefore reason that the function loss of the p.R29W mutation could be a result of altered dimerization. In family CHRO 319, we found the p.R29W mutation compound heterozygous with an exchange in intron 17, c.2144+1G>A. As shown in heterologous minigene splicing experiments, this mutation affects correct processing of the PDE6C transcript, resulting in a transcript with a frameshift and premature translational termination (Fig. 1B).

The missense mutation p.R104W was observed in family CHRO 573 homozygously, and represents a novel mutation. This mutation affects an evolutionary highly conserved residue within the first GAFa domain, a region of the protein that non-catalytically binds cGMP and regulates the activity of the enzyme. This mutation resulted in a complete loss of enzymatic function. Arginine 104 is part of a conserved interaction surface of PDE6C GAFa that consists of numerous negatively charged and hydrophobic residues and is likely to interact with the proline-rich polycationic region of Pγ (18). Beyond that, it has been shown that direct binding of the polycationic region of Pγ to the GAFa domain stabilizes the non-catalytic cGMP-binding sites (19). One could speculate that p.R104W affects Pγ binding, resulting in a decrease of cGMP affinity and thus leading to a destabilization of nucleotide binding.

The p.P391L substitution was found in family CHRO 403 diagnosed with complete ACHM, whereas the p.Y323N mutation was identified in a family with the incomplete type of this disease, indicating some residual cone function (14). Both mutations are located in the second regulatory GAFb domain (Fig. 2). The phenotypic difference between these patients is reflected by clear differences in cGMP hydrolysis activity of the two mutants. Whereas the p.P391L mutation

Table 2. Catalytic properties of wildtype and mutant chimeric PDE6C/PDE5 proteins

	K_m (M)	k_{cat} (mol cGMP mol PDE^{-1} s^{-1})	Zaprinast IC_{50} (M)	Pγ IC_{50} (nM)	PDE activity (%)
Wildtype	0.72 ± 0.19	0.12	2.9 ± 0.28	56 ± 0.16	100
Y323N	0.56 ± 0.06	0.035	8.1 ± 0.08	158 ± 0.3	22.3
E790K	0.53 ± 0.12	0.065	1.2 ± 0.16	2.7 ± 0.1	39.2
H602L	–	–	–	–	7.9
P391L	–	–	–	–	8.6
R104W	–	–	–	–	4.5
R29W	–	–	–	–	8.6

virtually abolished cGMP hydrolysis, the p.Y323N mutation retained residual enzymatic activity of 22.3% compared with the wildtype chimeric protein. In addition, the p.Y323N mutant was about 3-fold less sensitive for Pγ inhibition than the chimeric wildtype protein. These findings clearly indicate a correlation between the phenotypic outcome and functionality of the mutant chimeric proteins in our *in vitro* assays. Both mutations in the GAFb domain affect residues that are fully conserved among vertebrate PDE6 proteins. Yet so far, no crystal structure is available for the GAFb domain of PDE6C, which impedes the prediction of the effects of these mutations on the structure and function of this domain. The PDE2–GAFb crystal structure is the only suitable template to model PDE6C–GAFb, albeit a poor one, because of low homology between these two domains (20) (Fig. 6). In this model, Y323 is situated in a loop that has no PDE2 counterpart, thus making it difficult to predict the pathogenic effect. Nevertheless, our data for inhibition with Pγ suggests that Y323 contributes to the interaction with Pγ. In contrast, P391 is conserved in GAFa and GAFb domains of PDE2, PDE5 and PDE6 and, from the model, appears to be critical for GAFb folding.

Affected subjects in family CHRO 102 carry two *PDE6C* mutations p.H602L and p.E790K in compound heterozygous state (15). While the p.H602L mutant showed only baseline activity not significantly different from the untransfected control, we found that the p.E790K mutant still had considerable residual catalytic activity that reached approximately 40% of the wildtype. p.H602L affects the first histidine of the second metal-binding motif (Fig. 2), a common functional element of PDEs that complexes divalent cations as essential co-factors for PDE catalytic activity (21). Glutamate 790 is located adjacent to the Pγ binding site within the catalytic domain. The residual enzymatic activity of the p.E790K mutant prompted us to investigate further functional parameters of this mutant, notably its affinity for zaprinast, a catalytic-site inhibitor, and for Pγ. Inhibition by zaprinast was not altered significantly while Pγ inhibition was 20.7-fold more pronounced with an IC_{50} value of 2.7 nM compared with 56 nM for the wildtype protein. This apparent alteration in the affinity of the mutant PDE6C to Pγ may have a profound effect on the regulation of the catalytic activity under physiological conditions, in particular its activation by Tα•GTP under normal light conditions. In addition to its dual effect at the protein level, the mutation also impairs transcript processing owing to the fact that the nucleotide substitution affects the first nucleotide of exon 21. Applying a heterologous minigene splicing assay, we could show that approximately 40% of the mutant transcripts undergo irregular splicing by skipping exon 21 (15). Thus, this mutation exhibits a pleiotropic effect on transcript and protein level that—although quantitative in nature—is likely to sum up to a strong functional defect.

Up to now, 16 different *PDE6C* mutations have been identified in patients with autosomal recessive ACHM. Except for the p.R29W mutation, all other mutations were detected only in single families, suggesting a broad spectrum of low-prevalent *PDE6C* mutations in Caucasians. All patients examined in this study (seven families/12 affected patients) present with nystagmus, photophobia, poor visual acuity (BCVA 0.08–0.40) and total loss of color vision. In standard ERG recordings, cone function was not detectable, whereas rod responses were essentially normal. Ophthalmoscopy in these ACHM patients revealed normal retinal appearance or only minor macular changes, except for patient II:3 and II:4 of family CHRO 9 (15), which presented with an atrophy of the RPE in the macula, which is a typical feature for ACHM patients at 'endstages' (22). Hyperopia is common in patients with ACHM (10,23), though in our patients with *PDE6C* mutations refractive errors were quite variable, ranging from −8.00 to +6.00, with the majority of patients (5/7) being myopic (mean spherical equivalent −4.70). Transfoveal OCT scans showed an optical empty cavity in the fovea of approximately 250 μm in diameter with a corresponding defect of the RPE layer (Fig. 5). Additionally, in parafoveolar OCT scans, an irregular density of the photoreceptor layer was observed. These findings are typical for patients with ACHM (22).

All genes currently known to cause ACHM: *CNGA3*, *CNGB3*, *GNAT2* and *PDE6C* present crucial components of the cone phototransduction cascade. Together, these genes explain the majority (∼80%) of all ACHM cases in our patient collective of 492 independent patients and families. In half of the patients (48.2%), we found mutations in *CNGB3*, thus representing the main locus for this disease. In 28.7% of the cases *CNGA3* mutations were identified, and in a much lower percentage of 2.2% and 1.4%, mutations in *GNAT2* and *PDE6C*, respectively. These figures are derived from the by far largest patient sample investigated ($n = 492$) so far. These prevalences of the four genes involved in ACHM vary between patient groups of different geographic background: in the work of Thiadens and co-workers mutations in *CNGB3* account for 87%, *CNGA3* for 5% and *PDE6C* for less than 1%, while no mutations in *GNAT2* were found (13,14,24). But still, in 10–20% of the patients with ACHM, the genetic etiology remains unresolved.

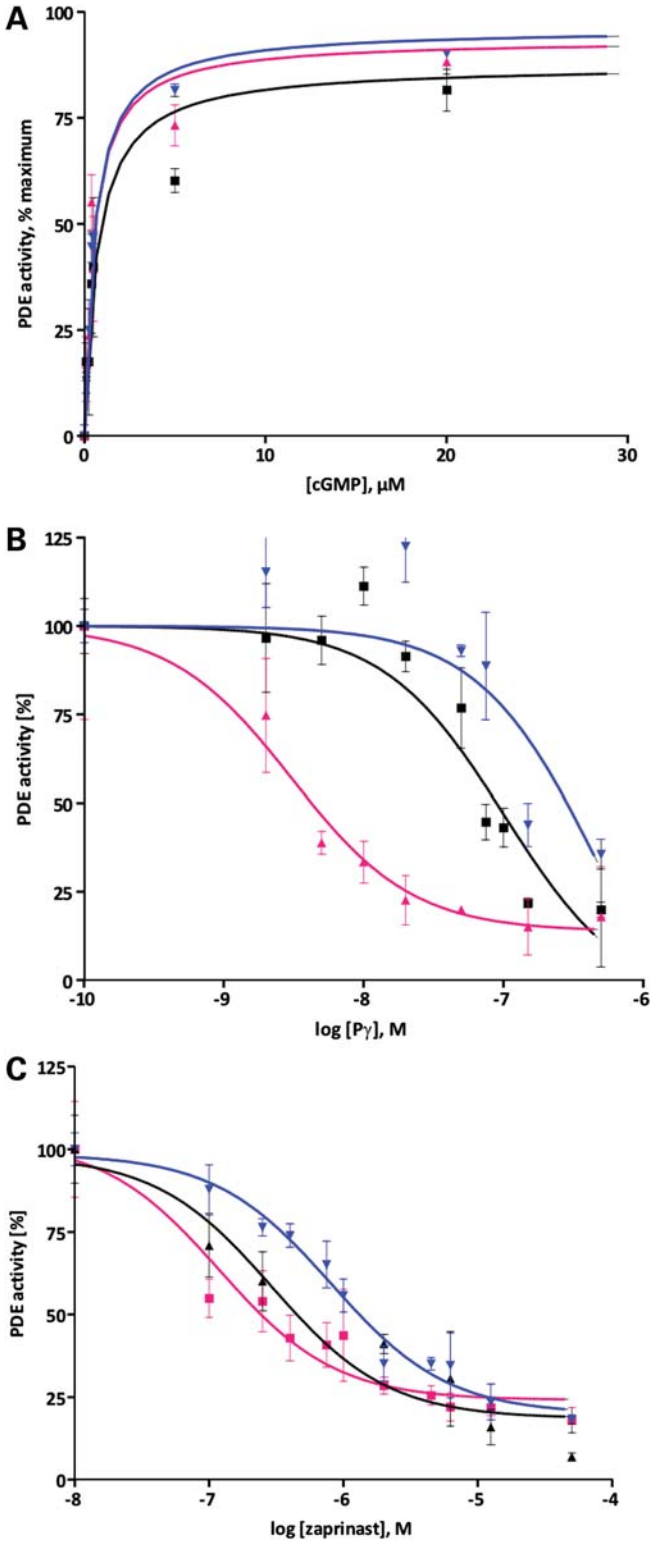

Figure 4. (**A**) Analysis of the substrate-binding properties of the chimeric wildtype (black, filled squares), the p.Y323N (blue, filled inverted triangles) and the p.E790K mutants (red, filled triangles). The rates of cGMP hydrolysis are expressed as percentage of maximal activity of the respective mutant PDE6C/PDE5. The K_m values of 0.72 ± 0.2 µM for chimeric wildtype, 0.53 ± 0.1 M for p.E790K and 0.56 ± 0.1 M for p.Y323N were calculated from the fitting curves. (**B**) Inhibition of cGMP hydrolysis of chimeric PDE6C/PDE5-wildtype, p.E790K and p.Y323N mutants with Pγ. The activities of chimeric wildtype (black, filled squares), p.E790K (red, filled triangles) and p.Y323N (blue, filled inverted triangles) mutant protein were determined in the presence of 5 M cGMP and increasing concentrations of Pγ, and are expressed as percentage of the respective PDE activity in the absence of Pγ. The calculated IC_{50} values are 56 ± 0.16 nM for wildtype, 2.7 ± 0.1 nM for the p.E790K mutant and 158 ± 0.3 nM for p.Y323N. (**C**) Inhibition of cGMP hydrolysis of chimeric PDE6C/PDE5 wildtype, p.E790K and p.Y323N mutants with zaprinast. Inhibition of cGMP phosphodiesterase activity by zaprinast. The rates of cGMP hydrolysis of chimeric wildtype (black, filled triangles), p.E790K (red, filled squares) and p.Y323N (blue, filled inverted triangles) mutant protein were determined in the presence of 5 M cGMP and increasing concentrations of zaprinast. The IC_{50} values of 2.9 ± 0.28 M for wildtype, 1.2 ± 0.16 M for p.E790K and 8.1 ± 0.08 M for p.Y323N mutant were calculated from the inhibition curves.

Several possibilities may be considered: A general problem in PCR-based screening protocols, as used in this study, is the failure to identify large genomic deletions and rearrangements. Yet, in our long-lasting analysis of these four genes, we have not observed any evidence that this is a common cause in these genes. Another possibility is that the missing mutations are located within introns or in upstream untranslated regulatory sequences, critical for splicing and expression. Such mutations may also account for the disease in the few subjects in which single heterozygous mutations have been found in either *CNGA3* or *CNGB3* (10,16). A third possibility is that at least a fraction of the unsolved cases are owing to mutations in as yet unknown genes, further increasing the genetic heterogeneity in ACHM.

MATERIALS AND METHODS

Patients, clinical examination and DNA isolation

Patients and family members were referred from different ophthalmological or medical genetic institutions and registered at the Molecular Genetics Laboratory, Institute for Ophthalmic Research, Tuebingen, Germany. The clinical diagnoses of ACHM or cone dysfunction were based on disease history, routine ophthalmological examinations, and varying specialized electrophysiological and psychophysical testing including scotopic and photopic ERG, visual acuity and color vision testing. Fundus examination included digital fundus photography and spectral-domain OCT.

The study was performed in accordance with the Declaration of Helsinki and received approval from the Ethical committee of the University of Tubingen. Patients were informed about the objectives of the study and consented to participate. Total genomic DNA was extracted from venous blood samples of patients and family members according to standard procedures.

PCR and sequencing-based *PDE6C* mutation screening

The 22 coding exons and their flanking intron boundaries of the *PDE6C* gene were amplified by PCR with genomic DNA as templates and subsequently used for DNA sequencing. PCR amplifications were performed in a total volume of 50 µl using a PCR mix containing 10 mM Tris pH 8.9, 50 mM KCl and 30 mM $MgCl_2$ or 10 mM Tris pH 8.3, 50 mM KCl, 1.5 mM $MgCl_2$ and 0.01% gelatine, 200 M of each dNTP, 10 pmol of each primer (Eurofins MWG Operon,

Table 3. Clinical findings in probands and affected relatives

Patient	*PDE6C* mutations	Diagnosis	Age of onset/ first diagnosis	Fundus/macular appearance	Cone ERG	Rod ERG	Photophobia	Nystagmus	BCVA (Best Eye)	Color Vision Defects	Involved color axis	Refractive error	Progression
CHRO 9/II:3	c.481-12T>A/ c.1483-2A>G	Complete ACHM	Congenital/ –	Atrophic RPE in the macula	Flat	Normal	Yes	congenital	0.10	severe	scotopic	OD: −8.00 OS: −7.38	n.d.
CHRO 9/II:4	c.481-12T>A/ c.1483-2A>G	Complete ACHM	Congenital/ –	Atrophic RPE in the macula	Flat	Normal	Yes	congenital	0.08	severe	scotopic	OD: −7.38 OS: −7.38	n.d.
CHRO 102/II:1	p.H602L/ p.E790K	ACHM	–/ 9 years	Granular	Flat	Normal	Yes	Yes	0.20	severe	n.d.	n.d.	n.d.
CHRO 102/II:2	p.H602L/ p.E790K	ACHM	–/ 7 years	Granular	Flat	Normal	Yes	Yes	0.20	severe	n.d.	n.d.	n.d.
CHRO 287/II:1	p.R276X/ p.Y819X	ACHM	–/ 6 months	No aberration	Flat	Normal	Yes	Yes	0.10	severe	n.d.	OD: +5.50 OS: +6.00	**No**
CHRO 319/II:1	p.R29W/ c.2144+1G>A	Complete ACHM	Congenital/ –	Normal with preserved foveal reflex	Flat	Normal	Yes	Yes	0.20	severe	scotopic	OD: −6.50 OS: −6.50	**No**
CHRO 403/II:1	p.P391L/ p.P391L	ACHM	Early childhood/ –	No aberration	Flat	Normal	Yes	Yes	0.20	severe	no interpretation possible	n.d.	n.d.
CHRO 403/II:2	p.P391L/ p.P391L	ACHM	Early childhood/ –	No aberration	Flat	Normal	Yes	Yes	0.20	severe	no interpretation possible	n.d.	n.d.
CHRO 403/II:3	p.P391L/ p.P391L	ACHM	Early childhood/ –	No aberration	n.d.	n.d.	Yes	Yes	0.40	n.d.	n.d.	n.d.	n.d.
CHRO 572/II:1	p.Y561X/ p.Y561X	ACHM	Congenital/ –	No aberration	Flat	Normal	Yes	congenital	0.20	severe	n.d.	OD: +4.25 OS: +5.75	n.d.
CHRO 573/II:1	p.R104W/ p.R104W	ACHM	–/ 3 months	Normal with preserved foveal reflex	Flat	Normal	Yes	congenital	0.10	severe	scotopic	OD: −0.75 OS: −0.75	**No**
CHRO 573/II:2	p.R104W/ p.R104W	ACHM	Congenital/ –	Normal with preserved foveal reflex	n.d.	Normal	Yes	congenital	0.10	n.d.	n.d.	OD: −1.50 OS: −1.00	**No**

BCVA, best-corrected visual acuity; n.d., no data.

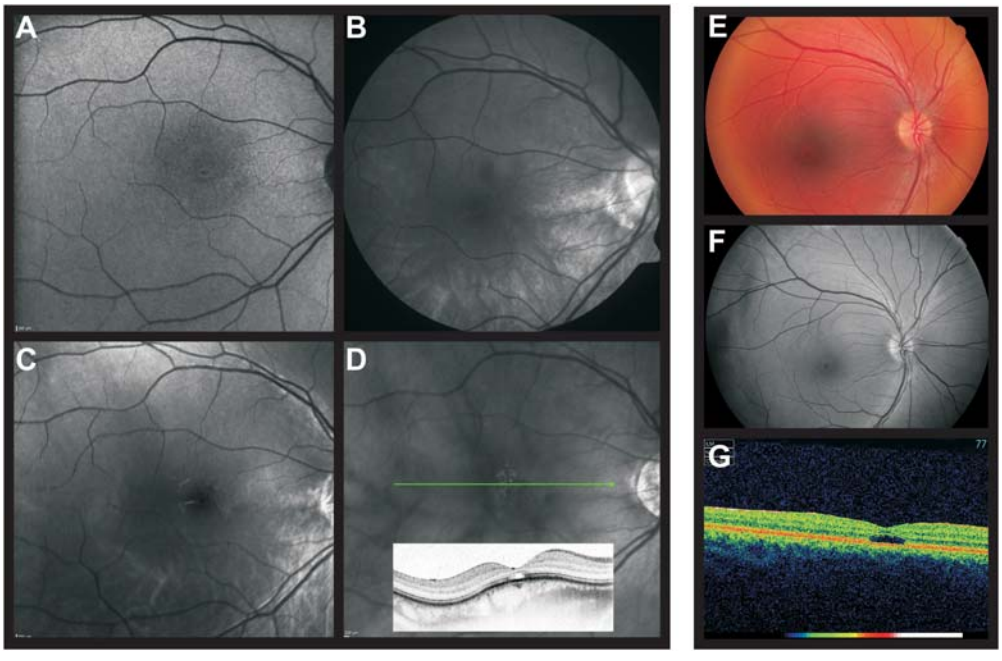

Figure 5. Fundus photography and OCT scans from a 33-year-old woman (CHRO 319/II:1) with compound heterozygous *PDE6C* mutations (c.85C>T/p.R29W and c.2144+1G>A) and high myopia (A–D), and a 14-year-old boy (CHRO 287/II:1) with compound heterozygous *PDE6C* mutations (c.826C>T/p.R276X and c.2457T>A/p.Y819X) (E-G). (**A**) Fundus autofluorescence (OD), (**B**) redfree (OD) and (**C**) blue 488 nm (OD) fundus photography were unremarkable, except for a pale, thin line around the foveola of the right eye on autofluorescence imaging. (**D**) Photoreceptor layer discontinuity and optically empty cavity in the center of the fovea (OD), (**E**) redfree (OD), (**F**) fundus photography showed a central cystic macular lesion and (**G**) OCT also showed an optical cavity in the center of the fovea. (A, B and D) Spectralis HRA + OC, Heidelberg Engineering GmbH, Heidelberg, Germany; (C) FF 450plus fundus camera, Carl Zeiss, Meditec AG, Jena, Germany; (E, F) Canon CF-60DSi digital fundus camera, Canon, Lake Success, New York, USA; (G) Topcon Mark II 3D OCT-1000, Topcon Deutschland GmbH, Willich, Germany.

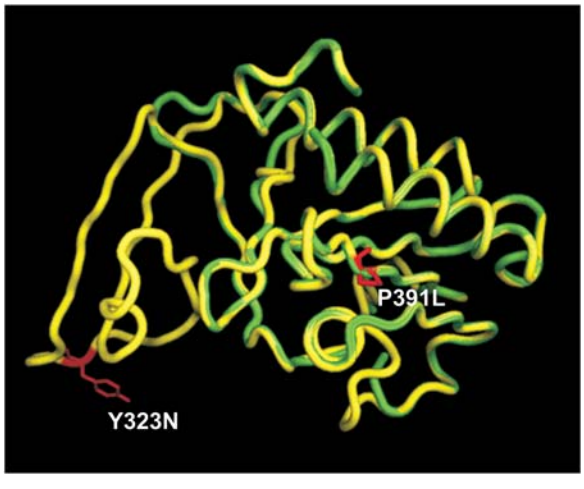

Figure 6. Molecular modeling of Y323 and P391 in the GAFb domain of PDE6C. A homology model of the PDE6C-GAFb domain was produced with SWISS-MODEL (28) using the coordinates of the PDE2-GAFb domain from the PDE2-GAFa-GAFb structure [PDB ID: 1MCO; (20)]. PDE6C-GAFb is shown in yellow and PDE2-GAFb in green. Y323 and P391 are displayed in red.

Ebersberg, Germany) (for primer sequences, see Supplementary Material, Table S1), 1 U AmpliTaq polymerase (Applied Biosystem, Weiterstadt, Germany) and 40–60 ng genomic DNA. Cycling parameters included initial denaturation at 94°C and elongation at 72°C for 5 min. Exon-specific annealing temperatures and number of cycles are listed in Supplementary Material, Table S2. PCR amplicons were purified with 1/20Vol. ExoSAP-IT (USB, Cleveland, OH, USA) in a 7 μl reaction mixture for 15 min at 37°C and then heat-denatured at 80°C for 15 min. Amplicons of the 22 coding exons and their flanking regions were sequenced in forward and reverse directions using the ABI PRISM Big Dye Terminator Cycle Sequencing Ready Reaction Kit (Perkin Elmer Applied Biosystem, Foster City, CA, USA) and separated on an ABI PRISM 3100 Genetic Analyzer (Applied Biosystems). The Lasergene Software package (DNASTAR, Lasergene Cooperation, London, UK) was used for editing and alignment of sequences.

Microsatellite analyses

Twelve families with at least two affected siblings were analyzed by marker segregation analysis for 11 different microsatellite markers: D2S113, D2S2311, D2S1897 and D2S388 linked to the *CNGA3* locus on chromosome 2q11.2; D8S167, D8S273 and D8S1838 linked to the *CNGB3* locus on chromosome 8q21-q22; D1S2651 and D1S495 linked to the *GNAT2* locus on chromosome 1p13.1; and D10S185 and D10S571 linked to the *PDE6C* locus on chromosome 10q24. Genotyping was performed by PCR amplification from genomic DNA, and fragment-sizing on an ABI PRISM 3100 Genetic Analyzer. Genotype calls were made using the Genescan software program.

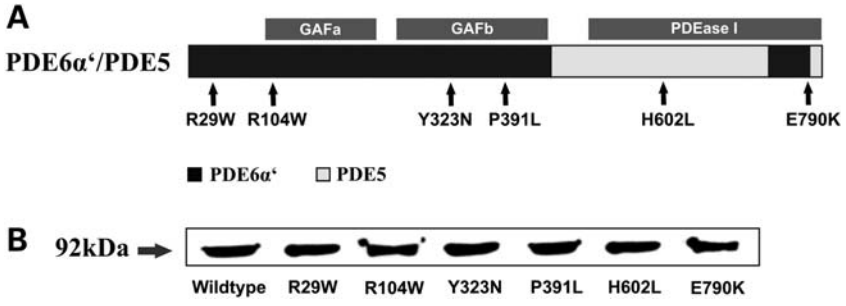

Figure 7. Structure and expression of chimeric PDE6C/PDE5 proteins in Sf9 insect cells. (**A**) Scheme of the PDE6C/PDE5 chimeric protein used for the functional studies. Localization of important functional domains of PDEs and the analyzed missense mutations are indicated. (**B**) Western blot analysis of purified recombinant PDE6C/PDE5 chimeric protein. 5 μg of purified protein was loaded per lane and detected using His-probe (H-15) rabbit polyclonal IgG (Santa Cruz).

Segregation analysis and exclusion in controls

Segregation analysis by DNA sequencing for the presence and independent inheritance of two mutant alleles were performed in all cases for which samples from additional family members were available. To evaluate the different identified missense sequence variations, we analyzed 200 healthy control samples (=400 chromosomes) for the following mutations: c.85C>T/p.R29W, c.310C>T/p.R104W, c.1172C>T/p.P391L, c.1805A>T/p.H602L and c.2368G>A/p.E790K. Analyses were carried out by PCR/restriction fragment length polymorphism for the mutations p.R29W, p.R104W and p.P391L using *Mwo*I, *Nci*I and *Hae*III, respectively. Single strand conformation polymorphism analyses were done for the mutations p.H602L and p.E790K. None of the mutations were observed in the control panel.

Heterologous splicing assay

To characterize the c.2144+1G>A mutation, a *PDE6C* gene segment covering the exons 16–18, including the entire internal introns and parts of the flanking intronic sequences, respectively, was amplified from genomic DNA applying Pfu Turbo polymerase (Stratagene, Amsterdam, Netherlands) and blunt-end cloned using the pCR-Script PCR Cloning Kit (Stratagene). This insert was excised by restriction enzyme digestion and reinserted into pSPL3_2096, a derivate of pSPL3 (Invitrogen Gmbh, Karlsruhe, Germany) with a stuffer fragment cloned into the original *Not*I site. Into this wildtype construct, the c.2144+1G>A mutation was introduced by *in vitro* mutagenesis (Quik Change *in vitro* Mutagenesis Kit, Stratagene). Wildtype and mutant constructs were partially sequenced, including the site of the mutation, the vector/insert and all exon/intron boundaries. COS7 cells were cultured in DMEM (PAA Laboratories GmbH, Pasching, Austria) supplemented with 5% (vol/vol) non-essential amino acids and 10% fetal calf serum (PAA). Cells were transfected with either mutant or wildtype pSPL3-PDE6C construct using Lipofectamine (Invitrogen). Total RNA was prepared 36 h post-transfection using TRIZOL reagent (Invitrogen), reverse-transcribed with SD6 and SA2, forward and reverse primers that are located in the 5′-tat and 3′-tat exons of the pSPL3 vector, respectively, and AMV reverse transcriptase (Takara RT–PCR Kit; Takara, Saint-Germain-en-Laye, France). The cDNA was amplified with pSPL3 exon primers, and RT–PCR products were directly sequenced.

Generation of chimeric PDE6C/PDE5 expression construct

We generated a 'humanized' PDE6C/PDE5-chimeric expression construct that comprises amino acid residues 1–445 and 741–790 of human PDE6C and residues 516–781 and 831–845 of human PDE5 (Fig. 7) analogous to the bovine expression construct Chi16 described previously (5,25). For construction, we employed the following plasmids: pXOP-human-PDE6C, pHis6-Chi8, pFastHTb-Chi16, pET15b-human-PDE5 and pFast-HTb-PDE5 (5,26). The $pHis_6$-hPDE6C-GAF construct was obtained by ligation of *Nco*I/*Hin*dIII as well as *Nco*I/*Eco*RI fragments of pXOP-human-PDE6C into pHis6-Chi8. The pFastHTb-Chi16/PDE5 construct was obtained by ligation of *Xho*I/*Hin*dIII fragment of pFastHTb-PDE5 as well as *Hin*dIII/*Spe*I fragment of human retinal RNA into pFastHTb-Chi16. The PDE5 fragment containing amino acids 831–845 was obtained using selected restriction sites and the pET15b-humanPDE5 as template and ligation into the pFastHTb-vector. After digestion with *Xho*I, *Hin*dIII, *Spe*I and *Nco*I, the fragments were ligated into the pFastHTb-Chi16 vector digested with the same enzymes. The mutations p.R29W (c.85C>T), p.R104W (c.310C>T), p.Y323N (c.967T>A), p.P391L (c.1172C>T), p.H602L (c.1805A>T) and p.E790K (c.2368G>A) were introduced by *in vitro* mutagenesis (Quik Change *in vitro* Mutagenesis Kit, Stratagene). The sequences of all PDE6C/PDE5 chimeras, wildtype and mutants, were confirmed by DNA sequencing of both strands. All restriction enzymes were purchased from New England Biolabs (NEB, Frankfurt am Main, Germany).

Expression of PDE6C/PDE5 chimeras in the baculovirus/Sf9 insect cell system

Generation of recombinant bacmids, transfection of Sf9 insect cells and viral amplifications were carried out according to the manufacturers' recommendations (Invitrogen). Sf9 insect cells were cultured in Sf-900 II SFM (Invitrogen) supplemented with 10% fetal calf serum (PAA) and 1% penicillin/streptomycin (PAA). For protein expression, Sf9 insect cell cultures (3×10^6 cells/ml in a total volume of 400 ml) were infected with recombinant baculoviruses at MOI 3–5, harvested by centrifugation 72 h after infection and washed with 20 mM

Tris–HCl buffer (pH 8.0) containing 150 mM NaCl. Sf9 cell pellets were resuspended in 20 mM Tris–HCl buffer (pH 8.0) with 2 mM $MgSO_4$ supplemented with Complete Mini EDTA-free protease inhibitor cocktail (Roche Applied Science, Mannheim, Germany). Cell lysates were generated by sonication (10 min, 0.3 s pulse, 100% amplitude) using the ultrasonic processor UP100H (Hielscher Ultrasonics GmbH, Teltow, Germany) and cleared by centrifugation (70,000*g*, 90 min, 4°C). Recombinant proteins were purified by affinity chromatography on a His-bind resin (Novagen, Madison, WI, USA) as described earlier (5). Concentrations of total protein were determined using a Bradford assay (Bio-Rad Protein Assay, Bio-Rad, Munich, Germany) according to manufacturers' instructions. SDS–polyacrylamide gel electrophoresis was performed using NuPAGE 4–12% Bis–Tris Gels (Invitrogen). For Western immunoblotting, 5 μg of purified protein was separated on SDS–polyacrylamide gels, transferred to nitrocellulose (0.45 M, Trans-Blot Transfer Medium, Bio-Rad) and analyzed using a His-probe (H-15) rabbit polyclonal IgG (Santa Cruz Biotechnology, Heidelberg, Germany) at 1:3.000 dilution. The antigen–antibody complexes were detected using anti-rabbit (1:10.000; GE Healthcare, Munich, Germany) conjugated to horseradish peroxidase and ECL reagent (Thermo Scientific, Munich, Germany) (Fig. 7). Purified protein was dialyzed against 40% glycerol and stored at −20°C.

PDE activity and PDE inhibition

PDE activity was measured using [^{3}H]-cGMP (GE Healthcare) as described previously (27). Briefly, 5 μg purified wildtype and mutant protein, respectively, were incubated in a total volume of 40 μl of 20 mM Tris–HCl pH 8.0, 50 mM NaCl, 15 mM $MgSO_4$, 2 mM beta-mercaptoethanol, 0.1 M shrimp alkaline phosphatase and 5 M [^{3}H]cGMP (100.000 cpm) at room temperature. After addition of [^{3}H]-cGMP, the reaction was allowed to proceed for 10 min and was stopped by the addition of 0.5 ml AG1-X2 anion exchange resin (Bio-Rad) in a 20% bed volume suspension. Samples were incubated for 10 min with occasional vortexing and spun at 9000*g* for 2 min. Aliquots of 0.25 ml clear supernatant were removed and measured in a scintillation counter (Beckman LS 6000 Liquid Scintillation Counter, Beckman Coulter GmbH, Krefeld, Germany). Each approach was performed in triplicates. To determine K_m values for cGMP, PDE activity was measured using cGMP concentrations between 0.5 μM and 100 M and the data were fitted to the equation $Y = V_{max} \times X/(K_m + X)$. To determine IC_{50} values for Pγ inhibition and for inhibition by zaprinast, PDE activity was measured with 5 M [^{3}H]-cGMP in the presence of increasing concentrations of Pγ and zaprinast, respectively. Before addition of [^{3}H]-cGMP, the reaction was allowed to proceed for 15 min at room temperature. The IC_{50} values were calculated by fitting data to the following equation: $Y = T - (T - B)/(1 + 10\text{^}((X - \log K_i) \times \text{hill slope}))$, where T (top) is PDE activity in the absence of Pγ or zaprinast, B (bottom) is PDE activity at an infinite concentration of Pγ or zaprinast and X is the logarithm of total Pγ or zaprinast concentration. Fitting the experimental data to equations was performed with nonlinear least-squares criteria using GraphPad Prism 4.0 software (GraphPad Software, Inc., La Jolla, CA, USA). The K_m and IC_{50} values are expressed as mean ± S.E. for three independent measurements.

Statistical significance was determined by two-way ANOVA for cGMP hydrolytic activity with and without inhibition, using MYSTAT 12 Version 12.02.00 (SYSTAT Inc., Chicago, IL, USA). A two-tailed P-value < 0.05 was considered statistically significant (*), $P = 0.001–0.01$ very significant (**) and $P < 0.001$ extremely significant (***).

SUPPLEMENTARY MATERIAL

Supplementary Material is available at *HMG* online.

ACKNOWLEDGEMENTS

We thank all patients and family members for participation. We also thank Britta Baumann and Kimberly K. Boyd for expert technical assistance; Brandy Barren and Hakim Muradov for their extensive assistance in data collection.

Conflict of Interest statement. The authors declare no competing financial interests.

FUNDING

This work was supported by the Deutsche Forschungsgesellschaft KFO134-Ko2176/1-1.

REFERENCES

1. Arshavsky, V. (2002) Like night and day: rods and cones have different pigment regeneration pathways. *Neuron*, **36**, 1–3.
2. Conti, M. and Beavo, J. (2007) Biochemistry and physiology of cyclic nucleotide phosphodiesterases: essential components in cyclic nucleotide signaling. *Annu. Rev. Biochem.*, **76**, 481–511.
3. Francis, S.H., Corbin, J.D. and Bischoff, E. (2009) Cyclic GMP-hydrolyzing phosphodiesterases. *Handb. Exp. Pharmacol.*, **191**, 367–408.
4. Granovsky, A.E., Natochin, M., McEntaffer, R.L., Haik, T.L., Francis, S.H., Corbin, J.D. and Artemyev, N.O. (1998) Probing domain functions of chimeric PDE6alpha'/PDE5 cGMP-phosphodiesterase. *J. Biol. Chem.*, **273**, 24485–24490.
5. Granovsky, A.E. and Artemyev, N.O. (2000) Identification of the gamma subunit-interacting residues on photoreceptor cGMP phosphodiesterase, PDE6alpha'. *J. Biol. Chem.*, **275**, 41258–41262.
6. Granovsky, A.E. and Artemyev, N.O. (2001) A conformational switch in the inhibitory gamma-subunit of PDE6 upon enzyme activation by transducin. *Biochemistry*, **40**, 13209–13215.
7. Kohl, S., Marx, T., Giddings, I., Jägle, H., Jacobson, S.G., Apfelstedt-Sylla, E., Zrenner, E., Sharpe, L.T. and Wissinger, B. (1998) Total colour blindness is caused by mutations in the gene encoding the alpha-subunit of the cone photoreceptor cGMP-gated cation channel. *Nat. Genet.*, **19**, 257–259.
8. Kohl, S., Baumann, B., Broghammer, M., Jägle, H., Sieving, P., Kellner, U., Spegal, R., Anastasi, M., Zrenner, E., Sharpe, L.T. *et al.* (2000) Mutations in the CNGB3 gene encoding the beta-subunit of the cone photoreceptor cGMP-gated channel are responsible for achromatopsia (ACHM3) linked to chromosome 8q21. *Hum. Mol. Genet.*, **9**, 2107–2116.
9. Sundin, O.H., Yang, J.M., Li, Y., Zhu, D., Hurd, J.N., Mitchell, T.N., Silva, E.D. and Maumenee, I.H. (2000) Genetic basis of total colour blindness among the Pingelapese islanders. *Nat. Genet.*, **25**, 289–293.

10. Wissinger, B., Gamer, D., Jägle, H., Giorda, R., Marx, T., Mayer, S., Tippmann, S., Broghammer, M., Jurklies, B., Rosenberg, T. *et al.* (2001) CNGA3 mutations in hereditary cone photoreceptor disorders. *Am. J. Hum. Genet.*, **69**, 722–737.
11. Aligianis, I.A., Forshew, T., Johnson, S., Michaelides, M., Johnson, C.A., Trembath, R.C., Hunt, D.M., Moore, A.T. and Maher, E.R. (2002) Mapping of a novel locus for achromatopsia (ACHM4) to 1p and identification of a germline mutation in the alpha subunit of cone transducin (GNAT2). *J. Med. Genet.*, **39**, 656–660.
12. Kohl, S., Baumann, B., Rosenberg, T., Kellner, U., Lorenz, B., Vadalà, M., Jacobson, S.G. and Wissinger, B. (2002) Mutations in the cone photoreceptor G-protein alpha-subunit gene GNAT2 in patients with achromatopsia. *Am. J. Hum. Genet.*, **71**, 422–425.
13. Thiadens, A.A., Slingerland, N.W., Roosing, S., van Schooneveld, M.J., van Lith-Verhoeven, J.J., van Moll-Ramirez, N., van den Born, L.I., Hoyng, C.B., Cremers, F.P. and Klaver, C.C. (2009) Genetic etiology and clinical consequences of complete and incomplete achromatopsia. *Ophthalmology*, **116**, 1984–1989.
14. Thiadens, A.A., den Hollander, A.I., Roosing, S., Nabuurs, S.B., Zekveld-Vroon, R.C., Collin, R.W., De Baere, E., Koenekoop, R.K., van Schooneveld, M.J., Strom, T.M. *et al.* (2009) Homozygosity mapping reveals PDE6C mutations in patients with early-onset cone photoreceptor disorders. *Am. J. Hum. Genet.*, **85**, 240–247.
15. Chang, B., Grau, T., Dangel, S., Hurd, R., Jurklies, B., Sener, E.C., Andreasson, S., Dollfus, H., Baumann, B., Bolz, S. *et al.* (2009) A homologous genetic basis of the murine cpfl1 mutant and human achromatopsia linked to mutations in the *PDE6C* gene. *Proc. Natl Acad. Sci.*, **106**, 19581–19586.
16. Kohl, S., Varsanyi, B., Antunes, G.A., Baumann, B., Hoyng, C.B., Jägle, H., Rosenberg, T., Kellner, U., Lorenz, B., Salati, R. *et al.* (2005) CNGB3 mutations account for 50% of all cases with autosomal recessive achromatopsia. *Eur. J. Hum. Genet.*, **13**, 302–308.
17. Muradov, K.G., Boyd, K.K., Martinez, S.E., Beavo, J.A. and Artemyev, N.O. (2003) The GAFa domains of rod cGMP-phosphodiesterase 6 determine the selectivity of the enzyme dimerization. *J. Biol. Chem.*, **278**, 10594–10601.
18. Martinez, S.E., Heikaus, C.C., Klevit, R.E. and Beavo, J.A. (2008) The structure of the GAF A domain from phosphodiesterase 6C reveals determinants of cGMP binding, a conserved binding surface, and a large cGMP-dependent conformational change. *J. Biol. Chem.*, **283**, 25913–25919.
19. Muradov, K.G., Granovsky, A.E., Schey, K.L. and Artemyev, N.O. (2002) Direct interaction of the inhibitory gamma-subunit of Rod cGMP phosphodiesterase (PDE6) with the PDE6 GAFa domains. *Biochemistry*, **41**, 3884–3890.
20. Martinez, S.E., Wu, A.Y., Glavas, N.A., Tang, X.B., Turley, S., Hol, W.G. and Beavo, J.A. (2002) The two GAF domains in phosphodiesterase 2A have distinct roles in dimerization and in cGMP binding. *Proc. Natl Acad. Sci. USA*, **99**, 13260–13265.
21. He, F., Seryshev, A.B., Cowan, C.W. and Wensel, T.G. (2000) Multiple zinc binding sites in retinal rod cGMP phosphodiesterase, PDE6alpha beta. *J. Biol. Chem.*, **275**, 20572–20577.
22. Thiadens, A.A., Somervuo, V., van den Born, L.I., Roosing, S., van Schooneveld, M.J., Kuijpers, R.W., van Moll-Ramirez, N., Cremers, F.P., Hoyng, C.B. and Klaver, C. (2010) Progressive loss of cones in achromatopsia. An imaging study using spectral-domain optical coherence tomography. *Invest. Ophthalmol. Vis. Sci.*, **51**, 5952–5957.
23. Kelly, J.P., Crognale, M.A. and Weiss, A.H. (2003) ERGs, cone-isolating VEPs and analytical techniques in children with cone dysfunction syndromes. *Doc. Ophthalmol.*, **106**, 289–304.
24. Thiadens, A.A., Roosing, S., Collin, R.W., van Moll-Ramirez, N., van Lith-Verhoeven, J.J., van Schooneveld, M.J., den Hollander, A.I., van den Born, L.I., Hoyng, C.B., Cremers, F.P. *et al.* (2010) Comprehensive analysis of the achromatopsia genes *CNGA3* and *CNGB3* in progressive cone dystrophy. *Ophthalmology*, **117**, 825–830.
25. Muradov, K.G., Granovsky, A.E. and Artemyev, N.O. (2003) Mutation in rod PDE6 linked to congenital stationary night blindness impairs the enzyme inhibition by its gamma-subunit. *Biochemistry*, **42**, 3305–3310.
26. Muradov, H., Boyd, K.K., Haeri, M., Kerov, V., Knox, B.E. and Artemyev, N.O. (2009) Characterization of human cone phosphodiesterase-6 ectopically expressed in *Xenopus laevis* rods. *J. Biol. Chem.*, **284**, 32662–32669.
27. Natochin, M. and Artemyev, N.O. (2000) Mutational analysis of functional interfaces of transducin. *Methods Enzymol.*, **315**, 539–554.
28. Arnold, K., Bordoli, L., Kopp, J. and Schwede, T. (2006) The SWISS-MODEL Workspace: a web-based environment for protein structure homology modeling. *Bioinformatics*, **22**, 195–201.